Tropospheric carbonyl sulfide mass balance based on direct measurements of sulfur isotopes

Chen Davidson[a], Alon Amrani[a,1], and Alon Angert[a]

[a]The Institute of Earth Sciences, The Hebrew University of Jerusalem, 95701 Jerusalem, Israel

Edited by Mark Thiemens, University of California San Diego, La Jolla, CA, and approved December 29, 2020 (received for review September 26, 2020)

Robust estimates for the rates and trends in terrestrial gross primary production (GPP; plant CO_2 uptake) are needed. Carbonyl sulfide (COS) is the major long-lived sulfur-bearing gas in the atmosphere and a promising proxy for GPP. Large uncertainties in estimating the relative magnitude of the COS sources and sinks limit this approach. Sulfur isotope measurements ($^{34}S/^{32}S$; $\delta^{34}S$) have been suggested as a useful tool to constrain COS sources. Yet such measurements are currently scarce for the atmosphere and absent for the marine source and the plant sink, which are two main fluxes. Here we present sulfur isotopes measurements of marine and atmospheric COS, and of plant-uptake fractionation experiments. These measurements resulted in a complete data-based tropospheric COS isotopic mass balance, which allows improved partition of the sources. We found an isotopic ($\delta^{34}S \pm SE$) value of 13.9 ± 0.1‰ for the troposphere, with an isotopic seasonal cycle driven by plant uptake. This seasonality agrees with a fractionation of −1.9 ± 0.3‰ which we measured in plant-chamber experiments. Air samples with strong anthropogenic influence indicated an anthropogenic COS isotopic value of 8 ± 1‰. Samples of seawater-equilibrated-air indicate that the marine COS source has an isotopic value of 14.7 ± 1‰. Using our data-based mass balance, we constrained the relative contribution of the two main tropospheric COS sources resulting in 40 ± 17% for the anthropogenic source and 60 ± 20% for the oceanic source. This constraint is important for a better understanding of the global COS budget and its improved use for GPP determination.

carbonyl sulfide | sulfur isotopes | gross primary production | anthropogenic sulfur | oceanic sulfur

The Earth system is going through rapid changes as the climate warms and CO_2 level rises. This rise in CO_2 is mitigated by plant uptake; hence, it is important to estimate global and regional photosynthesis rates and trends (1). Yet, robust tools for investigating these processes at a large scale are scarce (2). Recent studies suggest that carbonyl sulfide (COS) could provide an improved constraint on terrestrial photosynthesis (gross primary production, GPP) (2–12). COS is the major long-lived sulfur-bearing gas in the atmosphere and the main supplier of sulfur to the stratospheric sulfate aerosol layer (13), which exerts a cooling effect on the Earth's surface and regulates stratospheric ozone chemistry (14).

During terrestrial photosynthesis, COS diffuses into leaf stomata and is consumed by photosynthetic enzymes in a similar manner to CO_2 (3–5). Contrary to CO_2, COS undergoes rapid and irreversible hydrolysis mainly by the enzyme carbonic-anhydrase (6, 7). Thus, COS can be used as a proxy for the one-way flux of CO_2 removal from the atmosphere by terrestrial photosynthesis (2, 8–11). However, the large uncertainties in estimating the COS sources weaken this approach (10–12, 15). Tropospheric COS has two main sources: the oceans and anthropogenic emissions, and one main sink–terrestrial plant uptake (8, 10–13). Smaller sources include biomass burning, soil emissions, wetlands, volcanoes, and smaller sinks include OH destruction, stratospheric destruction, and soil uptake (12). The largest source of COS to the atmosphere is the ocean, both as direct COS emission, and as indirect carbon disulfide (CS_2) and dimethylsulfide (DMS) emissions that are rapidly oxidized to COS (10, 16–20). Recent studies suggest oceanic COS emissions are in the range of 200–4,000 GgS/y (19–22). The second major COS source is the anthropogenic source, which is dominated by indirect emissions derived from CS_2 oxidation, mainly from the use of CS_2 as an industrial solvent. Direct emissions of COS are mainly derived from coal and fuel combustion (17, 23, 24). Recent studies suggest that anthropogenic emissions are in the range of 150–585 GgS/y (23, 24). The terrestrial plant uptake is estimated to be in the range of 400–1,360 GgS/y (11). Measurements of sulfur isotope ratios ($\delta^{34}S$) in COS may be used to track COS sources and thus reduce the uncertainties in their flux estimations (15, 25–27). However, the isotopic mass balance approach works best if the COS end members are directly measured and have a significantly different isotopic signature. Previous $\delta^{34}S$ measurements of atmospheric COS are scarce and there have been no direct measurements of two important components: the $\delta^{34}S$ of oceanic COS emissions, and the isotopic fractionation of COS during plant uptake (15, 25–27). In contrast to previous studies that used assessments for these isotopic values, our aim was to directly measure the isotopic values of these missing components, and to determine the tropospheric COS $\delta^{34}S$ variability over space and time.

Results and Discussion

Two Groups of Ambient Air Samples. We collected 89 air samples over 2 y of measurements (Feb 2018 to Mar 2020), from multiple locations around the world (*SI Appendix*, Table S1). The vast majority of our samples (90%) showed a COS concentration of 480 ± 60 ppt (mean ± STD, 1σ) which agrees with the National Oceanic and Atmospheric Administration (NOAA) 20-y global COS monitoring program's mean concentration of 480 ± 40ppt (data provided by the NOAA/Global Monitoring Division in

Significance

Assessment for large-scale photosynthesis-climate feedbacks is needed. Carbonyl sulfide (COS) is an emerging proxy for the terrestrial photosynthesis. This proxy is limited by uncertainties related to the magnitudes of COS sources and sinks. Here, we demonstrate measurement-based assessments for the isotopic signal of: tropospheric COS, marine and anthropogenic COS emissions, and the isotopic fractionation of COS by plant uptake. All of these resulted in an isotopic mass balance for the COS budget which gives an important constraint for its sources.

Author contributions: C.D., A. Amrani, and A. Angert designed research; C.D. performed research; A. Amrani and A. Angert contributed new reagents/analytic tools; C.D. analyzed data; and C.D., A. Amrani, and A. Angert wrote the paper.

The authors declare no competing interest.

This article is a PNAS Direct Submission.

[1]To whom correspondence may be addressed. Email: alon.amrani@mail.huji.ac.il.

This article contains supporting information online at https://www.pnas.org/lookup/suppl/doi:10.1073/pnas.2020060118/-/DCSupplemental.

Published February 5, 2021.

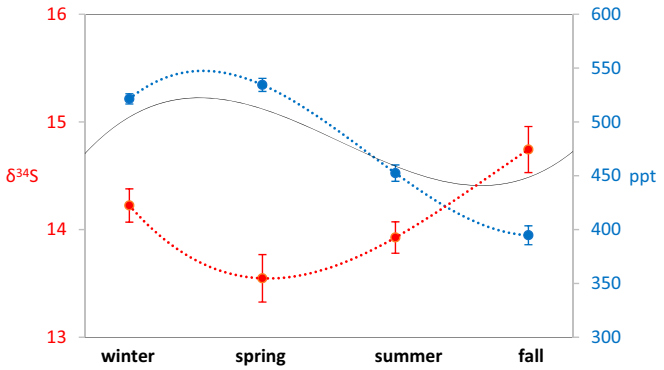

Fig. 1. The seasonal cycle in mean COS air concentration (blue) and $\delta^{34}S$ (red) for all ambient air samples taken in Israel by season (error bars represent SEs). The black line shows the best-fit line for 7 y monthly mean COS measurements at NOAA Mace Head station in Ireland (28).

Boulder, Colorado, USA, hereafter NOAA) (28). Yet 10% of our samples showed significantly higher concentrations that may indicate strong influence by local anthropogenic sources. Therefore, we divided our samples into two groups:

1) "Typical" air samples (COS concentration lower than 600 ppt; $n = 81$), normally distributed, with an average concentration of 480 ± 60 ppt and an average $\delta^{34}S$ value of 13.9 ± 0.8‰. This $\delta^{34}S$ value agrees with our previous estimate of tropospheric COS (15).
2) Air samples which are suspected to be strongly influenced by anthropogenic emissions (COS concentration higher than 600 ppt; $n = 8$) with an average COS concentration of 800 ± 200 ppt and an average $\delta^{34}S$ value of 11.6 ± 0.9‰. These values were not normally distributed, probably because of the small number of samples.

We will first discuss the typical air samples, and then the anthropogenic-influenced ones.

Seasonal Cycle in the Typical Air Samples. Our typical air samples show a seasonal cycle in COS concertation, with a mean of 530 ± 30 ppt for spring, and 400 ± 20 ppt for fall (P value = 4×10^{-12}) (Fig. 1). We also found an isotopic seasonal cycle for tropospheric COS, with a seasonal mean of 13.5 ± 1‰ ($\delta^{34}S$ ± STD) for spring and 14.7 ± 0.6‰ for fall (P value = 0.003) (Fig. 1). Analysis of all of our typical atmospheric air samples (not only from Israel) show a similar cycle in concentrations but a weaker apparent isotopic cycle with $\delta^{34}S$ values of 13.6 ± 1‰ for spring and 14.3 ± 1 for fall (P value = 0.02). The pronounced seasonal cycle of tropospheric COS concentrations agrees with previous studies in the Northern Hemisphere, most notably data collected at NOAA stations (2, 8, 12). For example, the NOAA Mace Head station in Ireland (MHD, 53°32′60″N/9°89′90″W) (28), is the closest to Israel, and as such may have similar COS concentrations. The NOAA MHD station shows a similar concentration cycle with a COS maximum of 520 ± 20ppt in spring and minimum of 440 ± 20 ppt in fall (Fig. 1 and *SI Appendix*, Table S2) (8). This seasonal cycle in the Northern Hemisphere is explained by the increased terrestrial photosynthesis during summer (2, 8, 10).

Plant-Uptake Isotopic Fractionation and the Seasonal Cycle. A seasonal cycle in COS $\delta^{34}S$ values is expected if plant uptake indeed dominates the COS concentration seasonal cycle, and if uptake of COS by plants is accompanied by an isotopic fractionation. We have previously estimated that this fractionation will be dominated by the effect of diffusion into plant stomata (15). This estimation was based on the fact that COS quickly reacts inside the leaf, and back-diffusion from the leaf to the atmosphere is minimal (6, 7). We have calculated, based on the theory of binary diffusion, a value of ε~−5‰ for this fractionation during plant uptake (15). Based on this theoretically estimated ε and the observed decrease in COS concentrations (130 ppt from spring to fall), the isotopic enrichment from fall to spring ($\Delta_{seasonal}$) is expected to be 1.5‰, using a Rayleigh distillation equation (which describes isotopic fractionation during continuous removal). However, our measurements show an isotopic enrichment of only 0.8‰ (all samples) to 1.2‰ (only samples from Israel), which may indicate a lower ε than the theoretically calculated value.

To directly measure the plant-uptake fractionation, we conducted plant-chamber experiments on a *Scindapsus aureus* branch (*Materials and Methods* and *SI Appendix*, Table S3). Plant-uptake fractionation (ε) was calculated using the concentrations and isotopic ratios of air samples before and after plant uptake in the chamber, using Rayleigh distillation (29). This calculation indicated a plant-uptake fractionation of (ε± SE) − 1.9 ± 0.3‰ (Fig. 2). While more work is needed to establish this value with more plant species, and under variable conditions, this value can be used as a preliminary direct estimate for terrestrial plant COS uptake fractionation. Combining this measured value of −1.9 ± 0.3‰ and our measured seasonal change in atmospheric COS concentration results in a calculated seasonal sulfur isotopic change of 0.6 ± 0.1‰ ($\Delta_{seasonal}$ ± SE), which is slightly lower than the measured value for all ambient air samples of 0.8‰. The difference between measured and calculated $\Delta_{seasonal}$ may be related to the neglection of smaller sources and sinks such as soil production or atmospheric destruction (via photolysis or OH reaction; *SI Appendix*). The $\Delta_{seasonal}$ for atmospheric samples from Israel alone is slightly higher (1.2‰), which may indicate the influence of additional processes, (e.g., anthropogenic and marine emissions) on the seasonal cycle.

Anthropogenic COS Influence on Ambient Air Samples. In addition to the seasonal variations, the typical air samples showed variability within the same season. This variability may be related to different sources and/or extent of anthropogenic COS contribution. To study this, we have analyzed the air-mass back-trajectories [produced by NOAA hybrid single-particle lagrangian integrated trajectory (HYSPLIT) Model (30)], and calculated anomalies versus the monthly mean, for all the air samples taken in Israel (*Materials and Methods*). The back-trajectories were divided

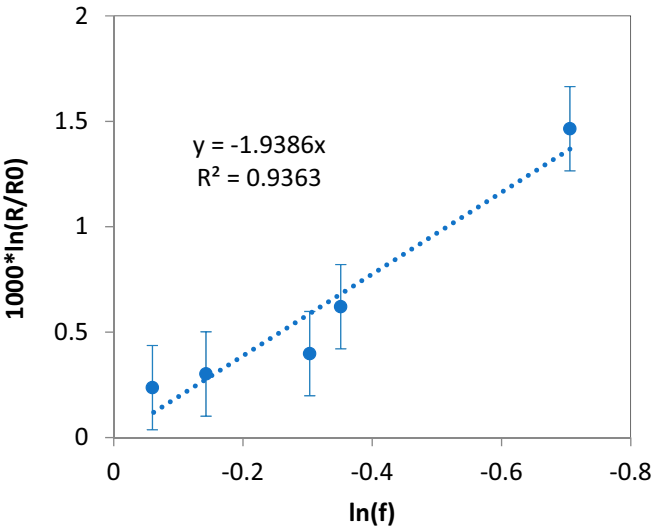

Fig. 2. Plant chamber experiments results on a Rayleigh distillation plot (29) indicate a plant-uptake fractionation of −1.9 ± 0.3‰. The error bars represent the analytical error.

into land-influenced air samples and sea-influenced air samples (*Materials and Methods* and *SI Appendix*, Fig. S3). We assumed that the land-influenced air samples will have positive COS concentration anomalies and negative $\delta^{34}S$ values anomalies due to anthropogenic activity. This analysis indicates a relationship between the back-trajectories and the COS concentration anomalies and supports our assumption of a distinct difference in concentrations between the two groups. The land-influenced back-trajectories' concentration anomalies were higher on average by 25 ppt than the sea-dominated ones (P value = 0.004) and the $\delta^{34}S$ values were lower by 0.4‰, on average (P value = 0.06). This may indicate that the typical samples are also slightly affected by regional anthropogenic emissions. Analysis of our air samples that showed strong anthropogenic influence (above 600 ppt), by an isotopic mixing line [or Keeling plot (31, 32)], presents a good fit to a linear trend line (R^2 = 0.61) (Fig. 3). This indicates an anthropogenic COS source with an isotopic value of 8 ± 1‰ ($\delta^{34}S$± SE). Taking this value and the observed 25-ppt difference between samples taken in Israel, with land-influenced and sea-influenced back-trajectories, predicted a lighter isotopic value ($\Delta_{land-sea}$) by 0.4‰ for the land-influenced air mass (Eq. 1):

$$\Delta_{land\text{-}sea} = \frac{[COS]_{land\text{-}influenced} - [COS]_{sea\text{-}influenced}}{[COS]_{land\text{-}influenced}} \times \delta^{34}S_{anthropogenic}, \quad [1]$$

where $\Delta_{land-sea}$ is the predicted isotopic difference between land-influenced and sea-influenced air masses; $[COS]_{land\text{-}influenced}$ is the mean COS concentration of air samples for which their back-trajectories indicate a land-influenced air mass; $[COS]_{sea\text{-}influenced}$ is the mean COS concentration of air samples for which their back-trajectories indicate a sea-influenced air mass; $\delta^{34}S_{anthropogenic}$ is the estimated isotopic signal for anthropogenic COS.

This $\Delta_{land-sea}$ prediction aligns with our air samples measurements: land-influenced back-trajectories' $\delta^{34}S$ values were lower by 0.4‰ on average (P value = 0.06), reinforcing our 8 ± 1% assessment for the anthropogenic COS isotopic signal. A recent estimate of ~5‰ for the anthropogenic isotopic signal was suggested by Hattori et al. (27) based on air samples from Japan. The relatively small ~3‰ difference between the two estimates may be related to different anthropogenic sources (i.e., the petrochemical industry in the Middle East versus rayon production and coal combustion in China), or to the different analytical methods used (15, 27).

Marine COS Sources $\delta^{34}S$ Analysis. We measured the concentration and $\delta^{34}S$ values of dissolved COS, CS_2, and DMS in seawater by using an air–water equilibrator (*Materials and Methods* and *SI Appendix*). We sampled seawater-equilibrated air at the Red Sea (May 2019; n = 6 and January 2020; n = 6) and the Mediterranean Sea (December 2019; n = 10) (sampling date, time, locations, and raw data are detailed in *SI Appendix*, Table S4). Table 1 summarizes the results of our three sampling campaigns. The DMS isotopic measurements from all sampling campaigns show a mean $\delta^{34}S$ value of 20 ± 1‰ (mean ± STD) in agreement with previous measurements (33). In contrast to DMS, the $\delta^{34}S$ values of COS and CS_2 show spatial and temporal variability (Table 1 and *SI Appendix*, Table S4), with an average (weighted by the concentrations) of 13 ± 3‰ and 15 ± 4‰ (mean ± STD), respectively. To calculate an estimate of COS $\delta^{34}S$ in global marine emissions, we used the weighted average $\delta^{34}S$ that we measured for each flux, together with average estimates from a recent review (12) of global COS fluxes. These fluxes include direct (130 GgS/y) and indirect emissions via CS_2 and DMS oxidation (135 and 40 GgS/y, respectively). This calculation resulted in an estimate of 14.7 ± 1‰ (weighted-mean± SE) for marine emissions, where the uncertainty is based only on the isotopic variability, and does not include uncertainty in the marine flux pathways. Since the direct COS and the CS_2-driven emissions have similar $\delta^{34}S$ values, the uncertainty will be mostly driven by the relative contribution of the DMS pathway, which is expected to be better constrained in the near future by new experiments and modeling. Nevertheless, our estimate can be used as an initial assessment for the isotopic signal of COS of the marine source. This is under the assumption (that should be validated in further studies) of no fractionation in the oxidation processes. It should be also noted that both of our sampling locations are characterized as oligotrophic seas, with similar chlorophyll A concentrations typically lower than 0.4 μg/L (34, 35). Thus, our initial assessment of the seawater-emitted COS isotopic signal

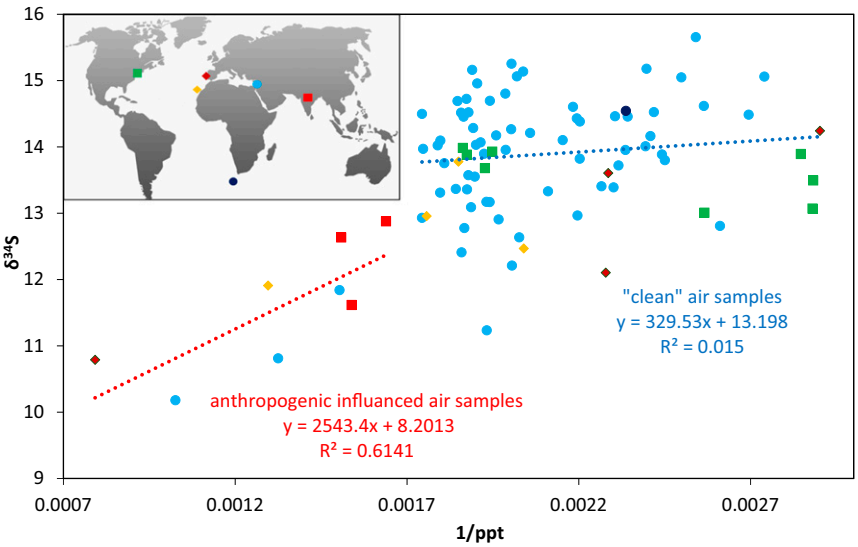

Fig. 3. Isotopic mixing lines (Keeling plot) for COS. The red trendline for the strongly anthropogenic-influenced samples (COS concentration above 600 ppt) indicates an anthropogenic COS source with an isotopic signal of 8 ± 1‰, while the blue line, which represents typical ambient air samples (COS concentrations below 600 ppt) does not show a pronounced trend. Samples were taken mostly in Israel (n = 69), but also in the Canary Island of Fuerteventura (n = 4), Harvard Forest, Massachusetts, USA (n = 8), Cabo da Roca, Portugal (n = 4), Southern Ocean (n = 1), and New Delhi, India (n = 3). (*Inset*) Markers colors indicate the location shown on the map.

Table 1. Marine COS, CS_2, and DMS concentration and $\delta^{34}S$ values of air equilibrated with seawater

	COS			CS_2			DMS		
Campaign*	$\delta^{34}S$, ‰	Conc. (gas), ppb	Conc. (aq), pmol/L	$\delta^{34}S$, ‰	Conc. (gas), ppb	Conc. (aq), pmol/L	$\delta^{34}S$, ‰	Conc. (gas), ppb	Conc. (aq), pmol/L
1	13.4 ± 0.3	1.7 ± 0.1	38 ± 2	12 ± 0.4	0.38 ± 0.01	20.9 ± 0.3	19.6 ± 0.4	8.5 ± 0.6	4,100 ± 300
2	16 ± 0.6	0.8 ± 0.2	17 ± 4	16.2 ± 0.9	0.18 ± 0.02	10.1 ± 0.8	20.5 ± 0.5	1 ± 0.1	520 ± 70
3	11 ± 0.5	1.2 ± 0.2	27 ± 3	18 ± 1	0.3 ± 0.06	17 ± 3	21.0 ± 0.4	2.9 ± 0.2	1,390 ± 80

*1, Red Sea (May 2019; $n = 6$); 2, Mediterranean Sea (December 2019; $n = 10$); and 3, Red Sea (January 2020; $n = 6$).
Values are given as mean ± SE. Concentrations are given in the measured gas-phase – conc. (gas) and in the calculated aqueous phase – conc. (aq).

may not be representative of the global oceans (further discussed in *SI Appendix*).

Isotopic Mass Balance and the COS Tropospheric Budget. Based on all of the above, we created a measurement-based isotopic mass balance for tropospheric COS (Eq. **2** and Fig. 4):

$$A \times \delta^{34}S_{anthropogenic} + O \times \delta^{34}S_{ocean} = P \times \left(\delta^{34}S_{ambient\ air} + \varepsilon_{plant\ uptake}\right), \quad [2]$$

where A is the anthropogenic source flux; $\delta^{34}S_{anthropogenic}$ is the anthropogenic source isotopic signal; O is the oceanic source flux; $\delta^{34}S_{ocean}$ is the oceanic source isotopic signal; P is the terrestrial plant-uptake flux; $\varepsilon_{plant\ uptake}$ is the fractionation by plant uptake; and $\delta^{34}S_{ambient\ air}$ is the isotopic mean value of tropospheric ambient air samples.

This simplified mass balance contains the two main sources (anthropogenic and oceanic) of the tropospheric COS and one main sink (terrestrial plant uptake) and assumes steady state (Eq. **3**):

$$A + O = P. \quad [3]$$

Smaller sources and sinks like stratospheric oxidation and soils (*SI Appendix*) were neglected. From Eqs. **2** and **3** above, one can derive Eq. **4**:

$$\frac{A}{P} = \frac{\delta^{34}S_{ambient\ air} + \varepsilon_{plant\ uptake} - \delta^{34}S_{ocean}}{\delta^{34}S_{anthropogenic} - \delta^{34}S_{ocean}}. \quad [4]$$

Using Eq. **4** and with our measured values, we calculated that the relative contribution of the anthropogenic source to the atmosphere is 40 ± 17% and that of the oceanic source is 60 ± 20%. Taking the most recent anthropogenic COS inventory of 405 ± 180 GgS/y (24), together with our constraint, invokes a large oceanic source of 600 ± 400 GgS/y, in agreement with recent studies (10, 19, 20). Our constraint is an improvement over previous studies of the global COS budget with uncertainties on flux estimates of up to 4- and 20-fold for the anthropogenic and oceanic sources, respectively (19–24). Recently, optimized values, with lower uncertainties, of 830 ± 150 GgS/y for the oceanic source and 350 ± 40 GgS/y for the industrial source, based on Monte Carlo simulations, were suggested by Campbell et al. (11). These optimized values lead to a relative contribution of 30 ± 5% and 70 ± 16% for the anthropogenic and oceanic sources, respectively, which agrees with our independent estimate within error.

The uncertainty in our assessment is mostly affected by the uncertainty of the ocean and anthropogenic isotopic signatures. In future work, we intend to conduct oceanic and anthropogenic sampling campaigns, COS hydrolysis experiments, and CS_2/DMS oxidation experiments in order to reduce uncertainties and better understand COS production processes.

To conclude, we showed that a measurement-based isotopic mass balance of COS end members can be used as a powerful, simple, and independent tool to constrain the tropospheric COS budget. We expect that in the future, such improved constraints on the COS budget will lead to better estimates of global and regional GPP and thus to more accurate models of plant-climate feedbacks.

Materials and Methods

Reagents and Standards. A Tenax resin (TA, 60–80 mesh; Sigma-Aldrich) was used to preconcentrate air and marine samples. Sulfur hexafluoride (SF_6, 500 ppm in helium) was purchased from Praxair and was used as internal standard in each analysis. Six standard volatile sulfur compounds in He ~21 ppm ("Mix 1;" H_2S, COS, methanethiol, ethanethiol CS_2, DMS) were purchased from Air Liquide America and were used for the final calibration of sample

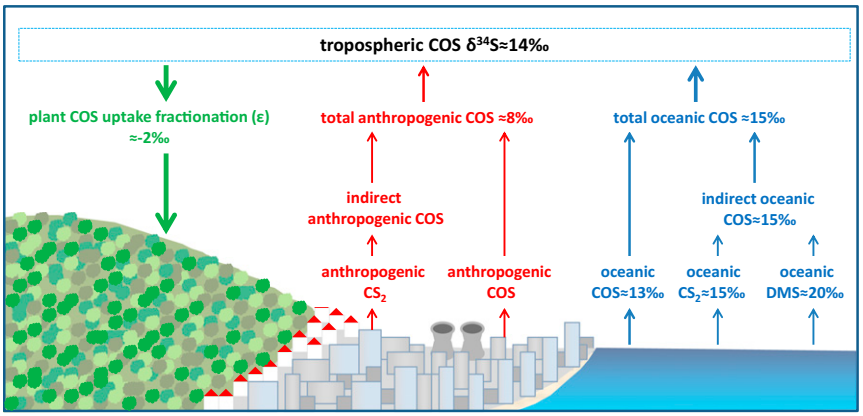

Fig. 4. A simplified tropospheric COS isotopic mass balance containing only the two main sources (anthropogenic and oceanic) and one main sink (terrestrial plant uptake).

concentrations and $\delta^{34}S$ values (15, 36). The $\delta^{34}S$ values of the Mix 1 compounds were calibrated against in-house liquid standards DMS (>99%; −3.0 ± 0.1‰), CS_2 (>99%; 17.2 ± 0.1‰) and thiophene (>99%; 9.6 ± 0.2‰), purchased from Sigma-Aldrich, that were isotopically calibrated as described previously (36). A COS 4.7% standard in helium (−6.2‰, calibrated against Mix 1) was purchased from Air Liquide America and was diluted to create two in-house standards (5.2 ppm in He and 1.7ppb in N_2 + 500 ppm CO_2) that were used to validate lack of fractionation and a full sample yield in the preconcentration process (15). The sulfur isotope reference materials NBS-127 ($BaSO_4$; $\delta^{34}S$ = 21.1‰), IAEA-S-1 (Ag_2S; −0.3‰), and IAEA-SO-6 ($BaSO_4$; −34.1‰) were purchased from NIST and were used for calibration of all the in-house liquid standards (36). All the $\delta^{34}S$ values in this work are reported against Vienna-Canyon Diablo Troilite (37).

Instrumentation. A preconcentration system connected to a gas chromatograph (GC, Trace 2000 series, Thermo, coupled with a Neptune Plus multicollector inductively coupled plasma mass spectrometer (MC-ICPMS; Thermo Scientific) was used to measure S isotopes of COS, CS_2, and DMS in air and marine samples. The precision and accuracy were ≤0.2‰ for COS $\delta^{34}S$ measurement of the 5.2-ppm (0.1 mL, ∼20 pmol per injection) in-house standard as described in Angert et al. (15), and ≤0.4‰ for air samples taken within the same hour. A full (>97%) COS recovery yield in the preconcentration system was validated with an in-house standard of 1.7 ppb COS, ∼500 ppm CO_2 and N_2 as balance gas as described in Angert et al. (15). The preconcentration system was composed of a 1.59-mm (inner diameter) × 3.18-mm (outer diameter) Teflon tube filled with 50 mg Tenax cooled by ethanol at −90 °C. A cold trap (ethanol at −40 °C) is used to remove water vapor. The Tenax trap is connected through a 6- or 10-way valve (Valco Instrument Co.) to a GC (in July 2019 we replaced the 6-port valve with a 10-port valve for a faster switch to calibration gas measurements). After ∼60 min when the pressure in the cylinder dropped to ∼115 kPa, (∼2 L airflow through) we heated the Tenax trap with boiling water to ∼100 °C, and injected the sample to the GC (∼30 to ∼40 pmol COS). The GC was equipped with a split/splitless injector for liquid injection of volatile samples and a heated (70 °C) six-port valve gas inlet system (Valco Instrument Co.) for the introduction of gaseous compounds with a computer-controlled actuator. The GC column (60 m × 0.320 mm, GS-GASPRO, Agilent Technologies) is able to separate cleanly between SO_2 or CS_2 and COS. A transfer line, heated to 200 °C, connected the GC to the plasma source (36). The S species were then atomized and ionized in the plasma source and yielded $^{32}S^+$ and $^{34}S^+$ ions that were transferred to the mass spectrometer unit of the GC/MC-ICPMS system for isotope ratio analysis (15). Data-processing procedure was as described in detail elsewhere (36, 38).

Air Sampling. For air sampling, we used vacuumed electropolished stainless-steel 3-L canisters and 3-L Silitek-treated canister (To-can and SilicoCan, Restek). First, we cleaned the canisters as described in Angert et al. (15). We repeated the cleaning procedure twice before each sampling to ensure clean canisters. After the second cleaning procedure, COS blanks were less than 1 pmol (∼3% of typical atmospheric COS samples) and in most cases were not detected at all. The clean cylinders then vacuumed to ∼0.005 ATM in the laboratory before sending the canisters to the sampling site. At the sampling site, we used a 100-mL syringe to flush a 0.5-μm stainless-steel filter (SS-4F-05) with fresh air, then we connected the filter to the canister and opened the canister valve for 3 min to ensure pressure equilibrium. The air was sampled through the filter to prevent aerosol contamination. In order to verify that the air samples were well preserved until analysis, we conducted a 2-mo preservation test (most samples were typically analyzed within 1 mo). Samples did not change significantly after 2 mo, compared to similar samples that were measured within 2–3 d, with P value = 0. 6 and 0.27 for COS $\delta^{34}S$ values and COS concentrations (*SI Appendix*, Table S1).

Marine Sampling. The system analyzes S compounds in the gas phase; therefore, dissolved gasses must be first extracted from the seawater onsite. The low COS concentration in seawater, less than 10–100 pmol·L^{-1} (12), requires relatively large water volume for a single isotopic analysis (∼0.2–2 L), which is hard to handle in a conventional purge and trap system. To avoid this, we used an equilibrator, which is a device that produces in its head space a flow of seawater droplets, in order to increase surface area for faster equilibration (39). The seawater is replaced constantly (an open system), but the air is trapped in the equilibrator and thus eventually reached equilibrium with the dissolved gasses in seawater according to Henry law. We used a laboratory-built 20-L poly(methyl methacrylate) equilibrator (*SI Appendix*, Fig. S1). During sampling, we covered the equilibrator with an opaque plastic sheet to eliminate photoproduction within the equilibrator. Seawater was inserted through a showerhead on the equilibrator's upper part, and an exit valve (diameter 1 in.) was connected in its lower part for draining water. A 1/8-in. tube was affixed to the top for sampling the equilibrated gas. We sampled the equilibrated gas after 1 to 2 h of water flow at a rate of 4–10 L/min (to ensure full equilibration, see *SI Appendix*), by closing the water exit valve, which forced the water level to rise and the equilibrated gas to flow through the sampling tube into a 5-L Tedlar sampling bag. The gas was immediately transferred into a cleaned and preevacuated 3-L Silitek-treated canister (as described in *Air Sampling*) in order to safely preserve the gas until analysis in the laboratory. In order to verify that the marine samples were well preserved until analysis, we conducted a 2-mo preservation test (most samples were typically analyzed within 1 mo). COS, CS_2, and DMS did not change significantly with P value ≥0.2 (see *SI Appendix* for details).

The conversion from the gas-phase concentration to the initial aqueous phase concentration was conducted using a temperature- and salinity-dependent function for the COS Henry constant (40). For DMS and CS_2 we used Henry constants of 4.8×10^{-1} and 5.5×10^{-2} M/atm, respectively (41).

Plant Fractionation Experiments. An *S. aureus* branch dipped in water (to eliminate soil microbial processes) sealed in a plant chamber was used for these experiments (*SI Appendix*, Fig. S2). The *S. aureus* is a resilient tropical C3 plant, chosen as a model plant because it can easily survive without soil (42). The plant chamber is a poly(methyl methacrylate), laboratory-made, cylinder with a magnetic fan on the top, for mixing the air inside the chamber, and an inflating Tedlar bag connected by a tube to the outside of the chamber so the air pressure inside will remain equal to atmospheric pressure during sampling. Sampling was done by opening a vacuumed canister connected to the filter and the chamber. A CO_2 sensor (GMP252, Vaisala) on top of the chamber was used to follow the CO_2 drawdown during an experiment. In each experiment we measured two air samples:

1) Ambient air: sampled right before we inserted the *S aureus* branch into the plant chamber.
2) Fractionated air: sampled after 1–3 h that the *S. aureus* plant consumed a fraction of the COS (and also CO_2) in the sealed chamber. The CO_2 concentration typically decreased during an experiment by 100–300 ppm (from the ∼400-ppm ambient concertation) depending on the duration of the experiment.

After analysis, plant-uptake fractionation (ε) was calculated using the concentrations and isotopic ratios of air samples before and after plant uptake in the chamber, assuming Rayleigh distillation. Results were plotted on a $-\ln(f)$ vs. $1{,}000 \cdot \ln(R/R_0)$ plot (29). The first sample (taken before we inserted the plant) was defined as the initial state, and the second sample (after 1–3 h, during which the plant consumed a fraction of the COS) was defined as the fractionated state. Before the experiment, we conducted the same procedure but without the plant as a blank. Both air samples were identical (only 10 ppt and 0.3‰ difference, within analytical error), meaning the chamber itself did not affect the experiment.

Back-Trajectory Analysis. The 50-d back-trajectories (produced by NOAA HYSPLIT model (30)) were divided into two groups: land-influenced air samples, in which the air mass passed near the surface over land (mostly the Middle East) before arriving at the sampling location, and sea-influenced air samples, in which the air mass passed near the Mediterranean Sea surface before arriving at the sampling location (*SI Appendix*, Fig. S3). We assumed that the land-influenced air samples would have a higher anthropogenic signal due to anthropogenic activity like the petrochemical industry. The analysis indicates a relationship between the back-trajectories and the COS anomalies, where these anomalies were defined as the deviation from a monthly mean concentration of "clean air" [based on 5-y monthly mean concentrations from the NOAA MHD monitoring station (28)], and seasonal mean $\delta^{34}S$ values (based on our seasonal mean $\delta^{34}S$ measurements). The summer measurements were not included in this analysis since all summer sample back-trajectories were sea influenced.

Data Availability. All study data are included in the article and/or *SI Appendix*

ACKNOWLEDGMENTS. We thank the collaborators who helped to collect atmospheric and marine samples and discussed the results: Sinikka Lennartz and Dennis Booge from GEOMAR Helmholtz Centre for Ocean Research Kiel; Jacob Silverman and Timor Katz from the Israel Oceanographic & Limnological Research; Asaf Rivlin from the Interuniversity Institute for Marine Sciences in Eilat; Tal Weiner from the Hebrew University of Jerusalem; and William Munger and Timothy Whitby from the US-Ha1 site whose operation is supported by the AmeriFlux Management Project with funding by the US Department of Energy's Office of Science under Contract DE-AC02-05CH11231,

and additionally is a part of the Harvard Forest Long Term Ecological Research site supported under contract by the NSF (DEB-1832210). We also thank the NOAA Air Resources Laboratory for the provision of the HYSPLIT transport and dispersion model, and the NOAA Global Monitoring Laboratory for the provision of COS concentration data used in this publication. We also thank Yigal Erel, Yeala Shaked, Dan Yakir, Alexandra Naor, and two anonymous reviewers for critical and constructive comments that greatly improve this paper. This research was partly funded by grants from the Israel Science Foundation (773/19, 1738/16). C.D. was partly supported by an award by the Women's League for Israel.

1. P. Friedlingstein *et al*., Uncertainties in CMIP5 climate projections due to carbon cycle feedbacks. *J. Clim.* **27**, 511–526 (2014).
2. J. E. Campbell *et al*., Photosynthetic control of atmospheric carbonyl sulfide during the growing season. *Science* **322**, 1085–1088 (2008).
3. L. Sandoval-Soto *et al*., Global uptake of carbonyl sulfide (COS) by terrestrial vegetation: Estimates corrected by deposition velocities normalized to the uptake of carbon dioxide (CO 2). *Biogeosciences* **2**, 125–132 (2005).
4. U. Seibt, J. Kesselmeier, L. Sandoval-Soto, U. Kuhn, J. Berry, A kinetic analysis of leaf uptake of COS and its relation to transpiration, photosynthesis and carbon isotope fractionation. *Biogeosciences* **7**, 333–341 (2010).
5. K. Stimler, S. A. Montzka, J. A. Berry, Y. Rudich, D. Yakir, Relationships between carbonyl sulfide (COS) and CO2 during leaf gas exchange. *New Phytol.* **186**, 869–878 (2010).
6. G. Protoschill-Krebs, J. Kesselmeier, Enzymatic pathways for the consumption of carbonyl sulphide (COS) by higher plants. *Bot. Acta* **105**, 206–212 (1992).
7. G. Protoschill-Krebs, C. Wilhelm, J. Kesselmeier, Consumption of carbonyl sulphide (COS) by higher plant carbonic anhydrase (CA). *Atmos. Environ.* **30**, 3151–3156 (1996).
8. S. Montzka *et al*., On the global distribution, seasonality, and budget of atmospheric carbonyl sulfide (COS) and some similarities to CO_2. *J. Geophys. Res. Atmos.* **112**, D09302 (2007).
9. D. Asaf *et al*., Ecosystem photosynthesis inferred from measurements of carbonyl sulphide flux. *Nat. Geosci.* **6**, 186 (2013).
10. J. Berry *et al*., A coupled model of the global cycles of carbonyl sulfide and CO2: A possible new window on the carbon cycle. *J. Geophys. Res. Biogeosci.* **118**, 842–852 (2013).
11. J. E. Campbell *et al*., Large historical growth in global terrestrial gross primary production. *Nature* **544**, 84–87 (2017).
12. M. E. Whelan *et al*., Reviews and syntheses: Carbonyl sulfide as a multi-scale tracer for carbon and water cycles. *Biogeosciences* **15**, 3625–3657 (2018).
13. C. Brühl, J. Lelieveld, P. J. Crutzen, H. Tost, The role of carbonyl sulphide as a source of stratospheric sulphate aerosol and its impact on climate. *ACPD* **11**, 20823–20854 (2011).
14. S. Solomon *et al*., The persistently variable "background" stratospheric aerosol layer and global climate change. *Science* **333**, 866–870 (2011).
15. A. Angert, W. Said-Ahmad, C. Davidson, A. Amrani, Sulfur isotopes ratio of atmospheric carbonyl sulfide constrains its sources. *Sci. Rep.* **9**, 741 (2019).
16. A. Kettle, U. Kuhn, M. Von Hobe, J. Kesselmeier, M. Andreae, Global budget of atmospheric carbonyl sulfide: Temporal and spatial variations of the dominant sources and sinks. *J. Geophys. Res. Atmos.* **107**, ACH 25-21–ACH 25-16 (2002).
17. M. Chin, D. Davis, Global sources and sinks of OCS and CS2 and their distributions. *Global Biogeochem. Cycles* **7**, 321–337 (1993).
18. D. J. Kieber, J. Jiao, R. P. Kiene, T. S. Bates, Impact of dimethylsulfide photochemistry on methyl sulfur cycling in the equatorial Pacific Ocean. *J. Geophys. Res. Oceans* **101**, 3715–3722 (1996).
19. T. Launois, S. Belviso, L. Bopp, C. Fichot, P. Peylin, A new model for the global biogeochemical cycle of carbonyl sulfide–Part 1: Assessment of direct marine emissions with an oceanic general circulation and biogeochemistry model. *Atmos. Chem. Phys.* **15**, 2295–2312 (2015).
20. L. Kuai *et al*., Estimate of carbonyl sulfide tropical oceanic surface fluxes using Aura tropospheric emission spectrometer observations. *J. Geophys. Res. Atmos.* **120**, 11012–11023 (2015).
21. S. T. Lennartz *et al*., Direct oceanic emissions unlikely to account for the missing source of atmospheric carbonyl sulfide. *Atmos. Chem. Phys.* **17**, 385–402 (2017).
22. S. T. Lennartz *et al*., The influence of dissolved organic matter on the marine production of carbonyl sulfide (OCS) and carbon disulfide (CS2) in the Eastern Tropical South Pacific. *Ocean Sci. Discussions* **15**, 1071–1090 (2019).
23. J. Campbell *et al*., Atmospheric carbonyl sulfide sources from anthropogenic activity: Implications for carbon cycle constraints. *Geophys. Res. Lett.* **42**, 3004–3010 (2015).
24. A. Zumkehr *et al*., Global gridded anthropogenic emissions inventory of carbonyl sulfide. *Atmos. Environ.* **183**, 11–19 (2018).
25. S. Hattori *et al*., Determination of the sulfur isotope ratio in carbonyl sulfide using gas chromatography/isotope ratio mass spectrometry on fragment ions 32S+, 33S+, and 34S+. *Anal. Chem.* **87**, 477–484 (2015).
26. K. Kamezaki, S. Hattori, E. Bahlmann, N. Yoshida, Large-volume air sample system for measuring 34 S/32 S isotope ratio of carbonyl sulfide. *Atmos. Meas. Tech.* **12**, 1141–1154 (2019).
27. S. Hattori, K. Kamezaki, N. Yoshida, Constraining the atmospheric OCS budget from sulfur isotopes. *Proc. Natl. Acad. Sci. U.S.A.* **117**, 20447–20452 (2020).
28. S. Montzka *et al*., Data from "NOAA ESRL Global Monitoring Laboratory, Boulder, Colorado, USA." https://esrl.noaa.gov/gmd/. Accessed 29 March 2020.
29. G. Dongmann, The contribution of land photosynthesis to the stationary enrichment of 18O in the atmosphere. *Radiat. Environ. Biophys.* **11**, 219–225 (1974).
30. A. F. Stein *et al*., NOAA's HYSPLIT atmospheric transport and dispersion modeling system. *Bull. Am. Meteorol. Soc.* **96**, 2059–2077 (2015).
31. C. D. Keeling, The concentration and isotopic abundances of atmospheric carbon dioxide in rural areas. *Geochim. Cosmochim. Acta* **13**, 322–334 (1958).
32. D. Pataki *et al*., The application and interpretation of Keeling plots in terrestrial carbon cycle research. *Global Biogeochem. Cycles* **17**, 1022 (2003).
33. A. Amrani, W. Said-Ahmad, Y. Shaked, R. P. Kiene, Sulfur isotope homogeneity of oceanic DMSP and DMS. *Proc. Natl. Acad. Sci. U.S.A.* **110**, 18413–18418 (2013).
34. N. Stambler, Bio-optical properties of the northern Red Sea and the Gulf of Eilat (Aqaba) during winter 1999. *J. Sea Res.* **54**, 186–203 (2005).
35. T. Katz *et al*., The first deep-sea mooring station in the eastern Levantine basin (DeepLev), outline and insights into regional sedimentological processes. *Deep Sea Res. Part II Top. Stud. Oceanogr.* **171**, 104663 (2020).
36. W. Said-Ahmad *et al*., Compound-specific sulfur isotope analysis of petroleum gases. *Anal. Chem.* **89**, 3199–3207 (2017).
37. H. R. Krouse, B. Tyler, Coplen. "Reporting of relative sulfur isotope-ratio data (technical report). *Pure Appl. Chem.* **69**, 293–296 (1997).
38. A. Amrani, A. L. Sessions, J. F. Adkins, Compound-specific δ34S analysis of volatile organics by coupled GC/multicollector-ICPMS. *Anal. Chem.* **81**, 9027–9034 (2009).
39. J. E. Johnson, Evaluation of a seawater equilibrator for shipboard analysis of dissolved oceanic trace gases. *Anal. Chim. Acta* **395**, 119–132 (1999).
40. V. S. Ulshöfer, G. Uher, M. O. Andreae, Evidence for a winter sink of atmospheric carbonyl sulfide in the northeast Atlantic Ocean. *Geophys. Res. Lett.* **22**, 2601–2604 (1995).
41. W. De Bruyn *et al*., Henry's law solubilities and Śetchenow coefficients for biogenic reduced sulfur species obtained from gas-liquid uptake measurements. *J. Geophys. Res. Atmos.* **100**, 7245–7251 (1995).
42. T. V. El-Mallakh, Y. Gao, R. S. El-Mallakh, The effect of simulated acid rain on growth of root systems of Scindapsus aureus. *Int. J. Plant Biol.* **5**, 5187 (2014).